Facile Mesophase Control of Periodic Mesoporous Organosilicas under Basic Conditions

Yucang Liang,[†] Egil Sev. Erichsen,[‡] Marianne Hanzlik,[§] and Reiner Anwander*,[†]

Department of Chemistry, University of Bergen, Allégaten 41, N-5007, Bergen, Norway, Laboratory for Electron Microscopy, University of Bergen, Allégaten 41, N-5007, Bergen, Norway, Institut für Technische Chemie, Technische Universität München, D-85747 Garching, Lichtenbergstraße 4, Germany

Received August 20, 2007. Revised Manuscript Received November 9, 2007

The mesophase structure of ordered periodic mesoporous organosilicas (PMOs) can be easily adjusted under basic conditions by variation of the sodium hydroxide concentration. PMOs with hexagonal (*p6mm*, two-dimensional pore system), cubic (*Pm3n* or *Fm3m*, three-dimensional cagelike pore system), and disordered hexagonal (MSU-type) symmetry were obtained from 1,2-bis(triethoxysilyl)ethane (BTEE)-derived synthesis gels in the presence of binary surfactant mixtures, $[CH_3(CH_2)_{15}NMe_3]^+Br^-$ ($C_{16}TABr$) and $[CH_3(CH_2)_nNMe_2(CH_2)_3NMe_3]^{2+}2Br^-$ ($n = 15, 17$), as structure-directing agents. With an increasing amount of NaOH, mesophase−mesophase transitions from *p6mm* → *Pm3n* → *Fm3m* → distorted cubic → MSU-type (3D-network of "wormholelike" mesopores) were evidenced by powder X-ray diffraction analysis and transmission electron microscopy. Slight variations of the NaOH concentration not only affected the PMO mesophase structure via the charge matching principle but also the PMO morphology. Among others, hexagons with smooth faces, regular decaoctahedrons, and spherical particles were found from scanning electron microscopy. The PMO mesophase was further found to be dependent on the carbon chain length of the surfactant. ^{13}C and ^{29}Si magic-angle-spinning NMR spectroscopy revealed that intact ethylene moieties were incorporated uniformly into the framework. According to N_2 physisorption measurements, the PMOs display Brunauer−Emmett−Teller surface areas as high as 870 m^2/g and cage diameters in the [55,63] Å size range. Finally, the hydrothermal stability of three representative PMOs with cubic *Pm3n*, cubic *Fm3m*, and hexagonal *p6mm* symmetry was investigated in detail.

Introduction

Surfactant-based supramolecular templating has attracted great attention for the synthesis of periodic mesoporous materials, comprising the M41S[1] and SBA-n[2] silica families, the MSU-n system,[3] aluminosilicates,[4] metal oxides,[5] aluminophosphates,[6] nonsilica materials,[7] carbon materials,[8] and inorganic–organic hybrid nanocomposites,[9] as well as organic–inorganic hybrid materials denoted as periodic mesoporous organosilicas (PMOs).[10–13] The mechanism of formation of purely siliceous periodic mesoporous materials has been investigated in detail. Extensive variations of the supramolecular template (surfactant type and mixtures), silica source, and synthesis parameters have contributed to a fundamental and comprehensive understanding of emerging mesophase transformations.[14–25] For PMOs, featuring organic

* Corresponding Author. Fax: +47 555 89490. E-mail: reiner.anwander@kj.uib.no.
[†] Department of Chemistry, University of Bergen.
[‡] Laboratory for Electron Microscopy, University of Bergen.
[§] Technische Universität München.

(1) (a) Kresge, C. T.; Leonowicz, M. E.; Roth, W. J.; Vartuli, J. C.; Beck, J. S. *Nature* **1992**, *359*, 710. (b) Beck, J. S.; Vartuli, J. C.; Roth, W. J.; Leonowicz, M. E.; Kresge, C. T.; Schmitt, K. D.; Chu, C. T. W.; Olson, D. H.; Sheppard, E. W.; McCullen, S. B.; Higgins, J. B.; Schlenker, J. L. *J. Am. Chem. Soc.* **1992**, *114*, 10834.
(2) (a) Huo, Q.; Margolese, D. I.; Ciesla, U.; Feng, P.; Gier, T. E.; Sieger, P.; Leon, R.; Petroff, P. M.; Schüth, F.; Stucky, G. D. *Nature* **1994**, *368*, 317. (b) Huo, Q.; Leon, R.; Petroff, P. M.; Stucky, G. D. *Science* **1995**, *268*, 1324. (c) Zhao, D.; Feng, J.; Huo, Q.; Melosh, N.; Fredrickson, G. H.; Chmelka, B. F.; Stucky, G. D. *Science* **1998**, *279*, 548. (d) Zhao, D. Y.; Huo, Q.; Feng, J.; Chmelka, B. F.; Stucky, G. D. *J. Am. Chem. Soc.* **1998**, *120*, 6024.
(3) (a) Tanev, P. T.; Chlbwe, M.; Pinnavaia, T. J. *Nature* **1994**, *368*, 321. (b) Bagshaw, S. A.; Prouzet, E.; Pinnavaia, T. J. *Science* **1995**, *269*, 1242. (c) Tanev, P. T.; Liang, Y.; Pinnavaia, T. J. *J. Am. Chem. Soc.* **1997**, *119*, 8616. (d) Kim, S. S.; Zhang, W.; Pinnavaia, T. J. *Science* **1998**, *282*, 1302.
(4) Liu, Y.; Zhang, W.; Pinnavaia, T. J. *J. Am. Chem. Soc.* **2000**, *122*, 8791.
(5) (a) Ying, J. Y.; Mehnert, C. P.; Wong, M. S. *Angew. Chem., Int. Ed.* **1999**, *38*, 56. (b) Grosso, D.; Soler-Illia, G. J. d. A. A.; Babonneau, F.; Sanchez, C.; Albouy, P.-A.; Brunet-Bruneau, A.; Balkenende, A. R. *Adv. Mater.* **2001**, *13*, 1085.
(6) (a) Oliver, S.; Kuperman, A.; Coombs, N.; Lough, A.; Ozin, G. A. *Nature* **1995**, *378*, 47. (b) Tiemann, M.; Fröba, M. *Chem. Mater.* **2001**, *13*, 3211.
(7) (a) Sayari, A.; Liu, P. *Microporous Mater.* **1997**, *12*, 149. (b) Schüth, F. *Chem. Mater.* **2001**, *13*, 3184. (c) He, X.; Antonelli, D. *Angew. Chem., Int. Ed.* **2002**, *41*, 214.
(8) (a) Liang, C.; Hong, K.; Guiochon, G. A.; Mays, J. W.; Dai, S. *Angew. Chem., Int. Ed.* **2004**, *43*, 5785. (b) Tanaka, S.; Nishiyama, N.; Egashira, Y.; Ueyama, K. *Chem. Commun.* **2005**, 2125. (c) Zhang, F.; Meng, Y.; Gu, D.; Yan, Y.; Yu, C.; Tu, B.; Zhao, D. *J. Am. Chem. Soc.* **2005**, *127*, 13508. (d) Meng, Y.; Gu, D.; Zhang, F.; Shi, Y.; Yang, H.; Li, Z.; Yu, C.; Tu, B.; Zhao, D. *Angew. Chem., Int. Ed.* **2005**, *44*, 7053. (e) Kosonen, H.; Valkama, S.; Nykänen, A.; Toivanen, M.; ten Brinke, G.; Ruokolainen, J.; Ikkala, O. *Adv. Mater.* **2006**, *18*, 201. (f) Liang, C.; Dai, S. *J. Am. Chem. Soc.* **2006**, *128*, 5316.
(9) (a) Stein, A.; Melde, B. J.; Schroden, R. C. *Adv. Mater.* **2000**, *12*, 1403. (b) Sayari, A.; Hamoudi, S. *Chem. Mater.* **2001**, *13*, 3151.
(10) Inagaki, S.; Guan, S.; Fukushima, Y.; Ohsuna, T.; Terasaki, O. *J. Am. Chem. Soc.* **1999**, *121*, 9611.
(11) (a) Asefa, T.; MacLachlan, M. J.; Coombs, N.; Ozin, G. A. *Nature* **1999**, *402*, 867. (b) Yoshina-Ishii, C.; Asefa, T.; Coombs, N.; MacLachlan, M. J.; Ozin, G. A. *Chem. Commun.* **1999**, 2539.
(12) Melde, B. J.; Holland, B. T.; Blanford, C. F.; Stein, A. *Chem. Mater.* **1999**, *11*, 3302.

10.1021/cm702359r CCC: $40.75
Published on Web 01/25/2008

groups/functionalities directly incorporated into the inorganic framework, most of the investigations focused on the synthesis and characterization of materials with hexagonal (*p6mm* or *P6*$_3$*/mmc*)[10–12] or cubic (*Pm3n*,[26,27] *Im3m*,[28–31] *Fm3m*,[32–35] or *Ia3d*)[36,37] symmetry by selecting cationic and neutral surfactants as well as copolymers as structure-directing agents and diverse organo-bridged alkoxysilanes $(R'O)_3Si\text{-}R\text{-}Si(OR')_3$ as organosilica precursors, under acidic or basic conditions. Less attention has been paid to PMO mesophase transformations emerging from distinct concentration profiles within a given surfactant/organosilica precursor/acid (base) mixture. Only a few articles discussed the implications of shape and concentration of surfactant molecules for the formation of different PMOs. Sayari et al. reported on the effect of the alkyl chain length of routinely used surfactant alkyltrimethylammonium chloride on the mesophase structure and pore size of PMOs.[38] Accordingly, only the mixture C_{16}TACl/1,2-bis(trimethoxysilyl)ethane (BTME) led to the formation of the cubic *Pm3n* mesophase. Inagaki and Kapoor showed the formation of either cubic or hexagonal mesophases of ethylene-bridged PMOs by altering the ratio of a surfactant mixture composed of cationic C_{18}TACl and nonionic $C_{12}(EO)_4$.[39] Kim et al. systematically investigated gemini surfactants $[C_nH_{2n+1}N(CH_3)_2(CH_2)_sN(CH_3)_2C_nH_{2n+1}]^{2+}2Br^-$ (n = 6–18 and s = 3–12; C_{n-s-n}) as templates giving access to ethylene-bridged PMOs with lamellar, bicontinuous cubic *Ia3d*, 2D hexagonal *p6mm*, 3D hexagonal *P6*$_3$*/mmc*, and cubic *Pm3n* symmetry under the same basic conditions.[37] Our previous reports on ethylene-bridged PMOs demonstrated that the concentration of the divalent cationic surfactant $[C_{16}H_{33}N(CH_3)_2(CH_2)_3N(CH_3)_3]^{2+}2Br^-$ (C_{16-3-1}) or of mixtures of cationic surfactants $[CH_3(CH_2)_{17}NMe_3]^+Br^-$ (C_{18}TABr) and $[CH_3(CH_2)_{17}NMe_2(CH_2)_3NMe_3]^{2+}2Br^-$ (C_{18-3-1}) strongly influenced the mesophase structure.[33,40] In a preliminary study, we also discovered that the base (NaOH) concentration affects the assembly of C_{16-3-1} molecules causing mesophase transformations: amorphous → hexagonal *p6mm* → cubic *Fm3m* → hexagonal *p6mm* symmetry.[33] Particularly, concentration profiles in binary surfactant mixtures seem to facilitate mesophase transformations between different cagelike structures.[33,40]

Mesoporous materials featuring large cavities which are 3D-interconnected by smaller windows facilitate the size-(shape)-selective diffusion of molecules compared to 2D hexagonal materials with channel-like pore configuration and, therefore, seem to be of high relevance for separation processes[41] and size-selective heterogeneous catalysis.[42–44] Linked to this, cagelike PMOs might receive special attention because they readily accommodate larger cage and window sizes compared to their periodic mesoporous silica (PMS) congeners.[44] Table 1 comprises cagelike PMOs, briefly addressing selected synthesis parameters.

Herein, we wish to report that the system BTEE/(C_{n-3-1} and C_{16}TABr) (BTEE = 1,2-bis(triethoxysilyl)ethane; n = 16, 18) gives access to well-ordered, morphologically distinct, and hydrothermally stable ethylene-bridged periodic mesoporous organosilicas with hexagonal *p6mm*, cubic *Pm3n*, and face-centered-cubic *Fm3m* symmetry as well as disordered mesophases such as 3D-interconnected networks of wormholelike mesostructures (*MSU-type*), simply by careful variation of the base concentration.

(13) (a) Hatton, B.; Landskron, K.; Whitnall, W.; Perovic, D.; Ozin, G. A. *Acc. Chem. Res.* **2005**, *38*, 305. (b) Hoffmann, F.; Cornelius, M.; Morell, J.; Fröba, M. *Angew. Chem., Int. Ed.* **2006**, *45*, 3216.
(14) Vartuli, J. C.; Schmitt, K. D.; Kresge, C. T.; Roth, W. J.; Leonowicz, M. E.; McCullen, S. B.; Hellring, S. D.; Beck, J. S.; Schlenker, J. L.; Olson, D. H.; Sheppard, E. W. *Chem. Mater.* **1994**, *6*, 2317.
(15) (a) Israelachvili, J. N.; Mitchell, D. J.; Ninham, B. W. *J. Chem. Soc., Faraday Trans. 2* **1976**, *72*, 1525. (b) Huo, Q.; Margolese, D. I.; Stucky, G. D. *Chem. Mater.* **1996**, *8*, 1147.
(16) Luan, Z.; He, H.; Zhou, W.; Klinowski, J. *J. Chem. Soc., Faraday Trans.* **1998**, *94*, 979.
(17) Ryoo, R.; Joo, S. H.; Kim, J. M. J. *Phys. Chem. B* **1999**, *103*, 7435.
(18) (a) Tolbert, S. H.; Landry, C. C.; Stucky, G. D.; Chmelka, B. F.; Norby, P.; Hanson, J. C.; Monnier, A. *Chem. Mater.* **2001**, *13*, 2247. (b) Landry, C. C.; Tolbert, S. H.; Gallis, K. W.; Monnier, A.; Stucky, G. D.; Norby, P.; Hanson, J. C. *Chem. Mater.* **2001**, *13*, 1600. (c) Kim, J. M.; Sakamoto, Y.; Hwang, Y. K.; Kwon, Y.-U.; Terasaki, O.; Park, S.-E.; Stucky, G. D. *J. Phys. Chem. B* **2002**, *106*, 2552.
(19) (a) Che, S.; Kamiya, S.; Terasaki, O.; Tatsumi, T. *J. Am. Chem. Soc.* **2001**, *123*, 12089. (b) Che, S.; Lim, S.; Kaneda, M.; Yoshitake, H.; Terasaki, O.; Tatsumi, T. *J. Am. Chem. Soc.* **2002**, *124*, 13962.
(20) Liu, M.-C.; Sheu, H.-S.; Cheng, S. *Chem. Commun.* **2002**, 2854.
(21) Grosso, D.; Babonneau, F.; Soler-Illia, G. J. d. A. A.; Albouy, P.-A.; Amenitsch, H. *Chem. Commun.* **2002**, 748.
(22) Gross, A. F.; Yang, S.; Navrotsky, A.; Tolbert, S. H. *J. Phys. Chem. B* **2003**, *107*, 2709.
(23) Cagnol, F.; Grosso, D.; Soler-Illia, G. J. d. A. A.; Crepaldi, E. L.; Babonneau, F.; Amenitsch, H.; Sanchez, C. *J. Mater. Chem.* **2003**, *13*, 61.
(24) Ogura, M.; Miyoshi, H.; Naik, S. P.; Okubo, T. J. *Am. Chem. Soc.* **2004**, *126*, 10937.
(25) Kim, T.-W.; Kleitz, F.; Paul, B.; Ryoo, R. *J. Am. Chem. Soc.* **2005**, *127*, 7601.
(26) Guan, S.; Inagaki, S.; Ohsuna, T.; Terasaki, O. *J. Am. Chem. Soc.* **2000**, *122*, 5660.
(27) Sayari, A.; Hamoudi, S.; Yang, Y.; Moudrakovski, I. L.; Ripmeester, J. R. *Chem. Mater.* **2000**, *12*, 3857.
(28) Cho, E.-B.; Kwon, K.-W.; Char, K. *Chem. Mater.* **2001**, *13*, 3837.
(29) Guo, W.; Kim, I.; Ha, C.-S. *Chem. Commun.* **2003**, 2692.
(30) Zhang, Z.; Tian, B.; Yan, X.; Shen, S.; Liu, X.; Chen, D.; Zhu, G.; Zhao, D.; Qiu, S. *Chem. Lett.* **2004**, *33*, 1132.
(31) Grudzien, R. M.; Pikus, S.; Jaroniec, M. *J. Phy. Chem. B* **2006**, *110*, 2972.
(32) Matos, J. R.; Kruk, M.; Mercuri, L. P.; Jaroniec, M.; Asefa, T.; Coombos, N.; Ozin, G. A.; Kamiyama, T.; Teresaki, O. *Chem. Mater.* **2002**, *14*, 1903.
(33) (a) Liang, Y.; Hanzlik, M.; Anwander, R. *Chem. Commun.* **2005**, 525. (b) Liang, Y.; Hanzlik, M.; Anwander, R. *J. Mater. Chem.* **2005**, *15*, 3919.
(34) Zhao, L.; Zhu, G.; Zhang, D.; Di, Y.; Chen, Y.; Terasaki, O.; Qiu, S. *J. Phys. Chem. B* **2005**, *109*, 764.
(35) Zhou, X.; Qiao, S.; Hao, N.; Wang, X.; Yu, C.; Wang, L.; Zhao, D.; Lu, G. Q. *Chem. Mater.* **2007**, *19*, 1870.
(36) Zhang, Z.; Yan, X.; Tian, B.; Shen, S.; Chen, D.; Zhu, G.; Qiu, S.; Zhao, D. *Chem. Lett.* **2005**, *34*, 182.
(37) Lee, H. I.; Pak, C.; Yi, S. H.; Shon, J. K.; Kim, S. S.; So, B. G.; Chang, H.; Yie, J. E.; Kwon, Y.-U.; Kim, J. M. *J. Mater. Chem.* **2005**, *15*, 4711.
(38) Hamoudi, S.; Yang, Y.; Moudrakovski, I. L.; Lang, S.; Sayari, A. *J. Phys. Chem. B* **2001**, *105*, 9118.
(39) Kapoor, M. P.; Inagaki, S. *Chem. Mater.* **2002**, *14*, 3509.
(40) Liang, Y.; Hanzlik, M.; Anwander, R. *J. Mater. Chem.* **2006**, *16*, 1238.
(41) Pérez-Mendoza, M.; Gonzalez, J.; Wright, P. A.; Seaton, N. A. *Langmuir* **2004**, *20*, 9856.
(42) (a) Garcia-Bennett, A. E.; Williamson, S.; Wright, P. A.; Shannon, I. J. *J. Mater. Chem.* **2002**, *12*, 3533. (b) Kim, T.-W.; Ryoo, R.; Kruk, M.; Gierszal, K. P.; Jaroniec, M.; Kamiya, S.; Terasaki, O. *J. Phys. Chem. B* **2004**, *108*, 11480.
(43) Zapilko, C.; Liang, Y.; Anwander, R. *Chem. Mater.* **2007**, *19*, 3171.
(44) Zapilko, C.; Liang, Y.; Nerdal, W.; Anwander, R. *Chem.—Eur. J.* **2007**, *13*, 3169.

Table 1. Synthesis Parameters of Ordered Periodic Mesoporous Organosilicas (PMOs) with Cagelike Topology[a]

PMO	mesophase	precursor	surfactant(s) (additive)	ref
		Basic Conditions		
HMM-2	*P6₃/mmc*	BTME	C_{18}TACl	10
PMO[SBA-2]	*P6₃/mmc*	BTEE	$C_{16-6-16}$	37
HMM-3	*Pm3n*	BTME	C_{16}TACl	26
PMO[SBA-1]	*Pm3n*	BTME	C_{16}TACl	27
PMO[SBA-1]	*Pm3n*	BTME	C_{18}TACl and Brij30	39
PMO[SBA-1]	*Pm3n*	BTEE	C_{18-3-1} and C_{18}TABr	40
PMO[SBA-1]	*Pm3n*	BTEE	$C_{12-6-12}$ or $C_{14-6-14}$	37
PMO[KIT-5]	*Fm3m*	BTEE	C_{16-3-1}	33
		Acidic Conditions		
PMO[FDU-1]	*Fm3m*	BTEE	B50–6600	32
PMO[FDU-1]	*Fm3m*	BTME	F127 (KCl)	34
PMO[FDU-1]	*Fm3m*	BTME	F127 (KCl, TMB)	35
PMO[SBA-16]	*Im3m*	BTEE and TEOS	F127	28
PMO[SBA-16]	*Im3m*	BTME	F127 (K_2SO_4)	29
PMO[SBA-16]	*Im3m*	BTEE	P123	30
PMO[SBA-16]	*Im3m*	ICS and TEOS	F127 (NaCl)	31

[a] Abbreviations: BTME = $(CH_3O)_3SiCH_2CH_2Si(OCH_3)_3$; BTEE = $(CH_3CH_2O)_3SiCH_2CH_2Si(OCH_2CH_3)_3$; $C_nTAX = CH_3(CH_2)_{n-1}N(CH_3)_3X$ (X = Cl, Br); Brij30 = $CH_3(CH_2)_{11}(OCH_2CH_2)_4OH$; $C_{n-s-1} = CH_3(CH_2)_{n-1}N(CH_3)_2(CH_2)_sN(CH_3)_3$ 2X (X = Cl, Br); $C_{n-s-n} = CH_3(CH_2)_{n-1}N(CH_3)_2(CH_2)_sN(CH_3)_2(CH_2)_{n-1}CH_3$ 2X (X = Cl, Br); B50-600 = $HO(CH_2CH_2O)_{39}(CH_2CH_2CH(CH_3)O)_{47}(CH_2CH_2O)_{39}H$; F127 = $HO(CH_2CH_2O)_{106}(CH_2CH(CH_3)O)_{70}(CH_2CH_2O)_{106}$; P123 = $HO(CH_2CH_2O)_{20}(CH_2CH(CH_3)O)_{70}(CH_2CH_2O)_{20}H$; ICS = tris[3-(trimethoxysilyl)-propyl]isocyanurate.

Experimental Section

Chemicals. BTEE as a silica precursor from ABCR, hexadecyltrimethylammonium bromide (C_{16}TABr) as structure-directing agent from Aldrich, and sodium hydroxide from Merck-Schuchardt were used without further purification. Divalent surfactants N-(3-trimethylammonium-propyl)hexa(octa)decylammoniumdibromide, $[CH_3(CH_2)_{15}NMe_2(CH_2)_3NMe_3]^{2+}2Br^-$ (C_{16-3-1}), and $[CH_3(CH_2)_{17}NMe_2(CH_2)_3NMe_3]^{2+}2Br^-$ (C_{18-3-1}) were synthesized by reaction of hexadecyldimethylamine or octadecyldimethylamine with (3-bromopropyl)trimethylammonium bromide, respectively.

Synthesis. A typical synthesis (material **1**) consisted of the following: a mixture of C_{18-3-1} (2.12 g), C_{16}TABr (2.62 g), and NaOH (1.44 g) in warm deionized water (167 g) was stirred at ambient temperature to form a clear solution. BTEE (7.32 g) was added under vigorous stirring, and the stirring was continued for 24 h to afford a homogeneous solution. Heating this solution to 95 °C for 6 h brought about a white precipitate. Finally, the suspension was aged at 95 °C for 24 h in a polypropylene bottle. The final molar composition of the gel was 1:0.19:0.36:1.80:463 BTEE/C_{18-3-1}/C_{16}TABr/NaOH/H_2O. The resulting white product was recovered by suction filtration before cooling and dried at ambient temperature. A series of PMOs **2**−**6** was synthesized by varying the amount of NaOH, using an otherwise identical procedure. For PMOs **7** and **8**, C_{18-3-1} was replaced by C_{16-3-1}. Synthesis details are shown in Table 2. For all of the as-synthesized materials, the surfactant was removed by Soxhlet extraction.[33] Hexagonal PMO **9** was obtained as described previously.[40]

Hydrothermal Stability Test of PMOs. Solvent-extracted PMOs **2**, **3**, and **9** with different symmetry were treated hydrothermally in boiling water for 24, 72, and 144 h, respectively. Then, the solid product was recovered by suction filtration and dried at ambient temperature.

Characterization. The powder X-ray diffraction (PXRD) patterns of PMOs were collected on a Philips X'pert PRO diffractometer using monochromatic Cu Kα (λ = 1.5418 Å) radiation. Transmission electron micrographs (TEM) were obtained using a JEOL JEM2010 operated at 160 kV. For TEM observations, the samples were dispersed in ethanol (99.9%) using the ultrasonic method and loaded onto a carbon microgrid. Scanning electron microscopy (SEM) images were recorded on a JEOL JSM-5900LV microscope operated at an accelerating voltage of 15 kV. All SEM images reported here are representative of the corresponding material. Nitrogen gas adsorption–desorption isotherms were measured at 77.4 K on a Micromeritics ASAP 2020 system. Samples were degassed at 523 K for at least 4 h before measurements. The specific BET surface area was obtained from the nitrogen adsorption branch of the isotherm in the relative pressure range from 0.04 to 0.2.[45] The pore size distributions were calculated from the adsorption branches using the *Barrett–Joyner–Halenda* (BJH) model.[46] ^{13}C and ^{29}Si magic angle spinning (MAS) NMR spectra were obtained at ambient temperature on a Bruker AV300 instrument in a magnetic field of 7.04 T. The ^{13}C spectra were recorded using cross polarization and proton decoupling at a spinning speed of 7 kHz. The ^{29}Si NMR spectra were obtained by the application of single-pulse excitation with high-power proton decoupling at spinning speed of 7 kHz. In addition, the cage diameter of the cagelike PMOs was calculated using eq 1, which has been proposed by Ravikovitch and Neimark.[47]

$$D_{me} = a(6\epsilon_{me}/\pi\nu)^{1/3} \quad (1)$$

where D_{me} is the diameter of the cavity of a cubic unit cell of length a and ϵ_{me} is the volume fraction of a regular cavity; $\epsilon_{me} = \rho_v V_{me}/(1 + \rho_v V_{me})$, where ρ_v is the density of the organosilica wall that was assumed to be that of siliceous materials (2.2 g cm^{-3}); for cubic structures, ν is the number of cavities present in the unit cell (for *Pm3n* space group, ν = 8; for *Fm3m* space group, ν = 4). Cage diameters of PMOs with cubic symmetry are listed in Table 2.

Results and Discussion

Figure 1 shows the PXRD patterns of the surfactant-free PMOs **1**–**6** fabricated under basic conditions. For sample **1**, three diffraction peaks were observed and indexed as (100), (110), and (200) planes with *p6mm* symmetry, indicating a typical 2D hexagonal mesostructure. A TEM analysis of sample **1** revealed ordered arrays along the direction perpendicular to the pore axis and the direction of the pore axis (Figure 2). Sample **2** displays a long-range ordered cubic mesophase with *Pm3n* symmetry, which is similar to that of previously reported mesoporous silicas[2a,b,48] or periodic mesoporous organosilicas.[26,38] The PXRD pattern of **2** not only exhibits three well-resolved peaks in the range of $1° < 2\theta < 2°$ that can be indexed as the (200), (210), and (211) reflections but also five peaks assignable to the (222), (321), (400), (420), and (431) planes ($2° < 2\theta < 4°$). The cubic mesostructure could be corroborated by TEM analysis. Some representative images with [100] and [110] incidences are shown in Figure 3, demonstrating the long-range ordering of the 3D cubic arrays.[48] Nitrogen physisorption analysis showed type-IV isotherms for samples **1** (Supporting Infor-

(45) (a) Brunauer, S.; Emmett, P. H.; Teller, E. *J. Am. Chem. Soc.* **1938**, *60*, 309. (b) Sing, K. S. W.; Everett, D. H.; Haul, R. A. W.; Moscou, L.; Pierotti, R. A.; Rouquérol, J.; Siemieniewska, T. *Pure Appl. Chem.* **1985**, *57*, 603.
(46) Barrett, E. P.; Joyner, L. G.; Halenda, P. P. *J. Am. Chem. Soc.* **1951**, *73*, 373.
(47) Ravikovitch, P. I.; Neimark, A. V. *Langmuir* **2002**, *18*, 1550.
(48) Sakamoto, Y.; Kaneda, M.; Terasaki, O.; Zhao, D. Y.; Kim, J. M.; Stucky, G. D.; Shin, H. J.; Ryoo, R. *Nature* **2000**, *408*, 449.

Table 2. Synthesis Details and Important Pore Parameters of PMOs under Study

sample[a]	X[b]/10^{-3}	product mesophase	a[c]/Å	a_s(BET)[d]/ m^2g^{-1}	$V_{p,des}$[e]/cm^3g^{-1}	D_{me}[f]/Å	$d_{p,ads}$[g]/Å	$d_{p,des}$[h]/Å
1[i]	3.89	hexagonal (*p6mm*)	56	742	1.41		36	34
2[i]	5.10	cubic (*Pm3n*)	116	721	0.62	60	31	31
3[i]	5.62	cubic (*Fm3m*)	98	618	0.54	63	32	32
4[i]	6.69	cubic (*Fm3m*)	92	865	0.72	61	33	29
5[i]	7.37	distorted cubic		644	0.55		35	33
6[i]	9.43	wormhole like	65	373	0.31		29	27
7[j]	6.69	cubic (*Pm3n*)	111	640	0.48	55	31	28
8[j,k]	6.69	cubic (*Pm3n*)	111	616	0.48	55	31	28

[a] Ratio of binary surfactant C_{n-3-1}: C_{16}TABr: BTEE = 0.19:0.36:1 with the aging time set at 24 h. [b] X = molar ratio of $NaOH/H_2O$ that corresponds to 1 mol BTEE. [c] Cell parameter calculated from formulas $a = 2d_{100}/(3)^{1/2}$ (*p6mm* symmetry), $a = d_{210}(5)^{1/2}$ (*Pm3n* symmetry), and $a = d_{111}(3)^{1/2}$ (*Fm3m* symmetry). [d] Specific BET surface area. [e] BJH desorption cumulative pore volume of pores between d_P = 15 Å and 200 Å; all samples were pretreated at 250 °C in vacuo until the pressure was $<10^{-3}$ Torr. [f] Calculated from eq 1. [g] Pore diameter according to the maximum of the BJH pore size distribution calculated from the adsorption branch. [h] Pore diameter according to the maximum of the BJH pore size distribution calculated from the desorption branch. [i] $n = 18$. [j] $n = 16$. [k] Aging time = 72 h.

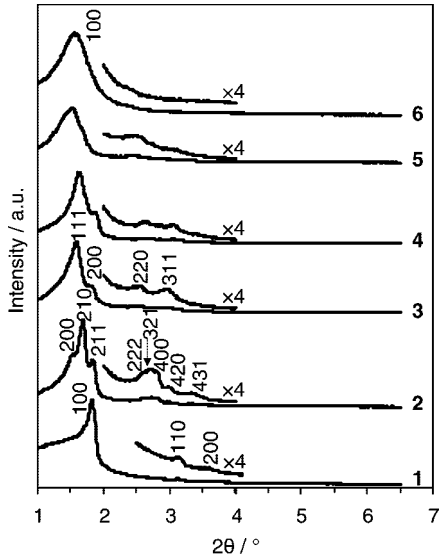

Figure 1. Powder X-ray diffraction patterns of solvent-extracted samples **1**–**6**.

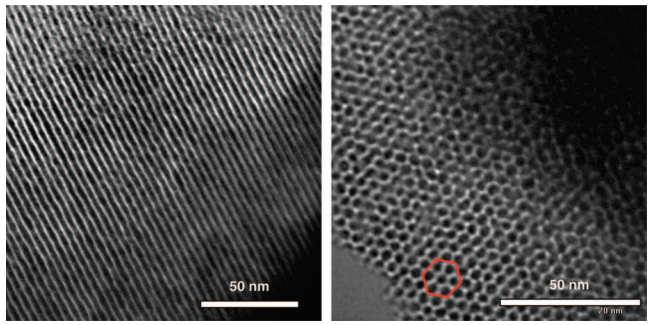

Figure 2. TEM images of the hexagonal PMO **1** with *p6mm* symmetry viewed along the direction perpendicular to the pore axis (left) and the direction of the pore axis (right).

mation (SI), Figure S1) and **2** (Figure 4), however, with distinct hysteresis loops. The H2 hysteresis loop found for sample **2** is characteristic of cagelike mesopores.[49] The pore volume of the hexagonal PMO **1** more than doubles that of the cubic mesophases obtained in this study (Table 2).

When the molar ratio of sodium hydroxide and water was adjusted carefully from 5.10×10^{-3} to 5.62×10^{-3}, 6.69×10^{-3}, 7.37×10^{-3}, and 9.43×10^{-3}, the obtained samples **3**–**6** underwent a remarkable mesophase transformation from *Pm3n* to *Fm3m* symmetry, then to a distorted cubic phase, and finally to an MSU-type structure. The PXRD patterns of the surfactant-extracted samples **3** and **4** showed four well-resolved diffraction peaks in the 2θ angle range of 1–4° (Figure 1), which were indexed as (111), (200), (220), and (311) reflection planes associated with face-centered cubic *Fm3m* symmetry. These patterns are in good agreement with those of previously reported purely siliceous materials KIT-5,[50,51] HOM-10,[52] and PMO[KIT-5].[33,34] For sample **4**, the TEM images clearly indicated a high, long-range ordering along the [100], [110], and [111] directions (Figure

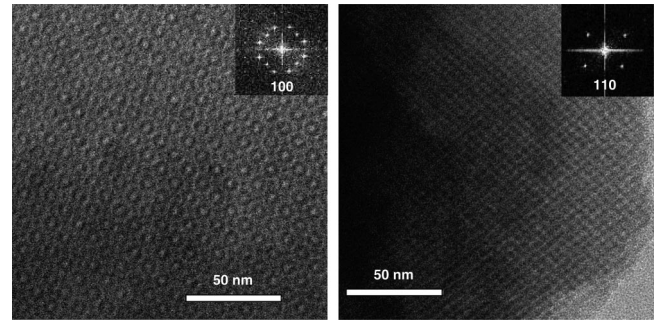

Figure 3. TEM images of the cubic PMO **2** with *Pm3n* symmetry along different directions [100] (left) and [110] (right), and their Fourier diffractograms.

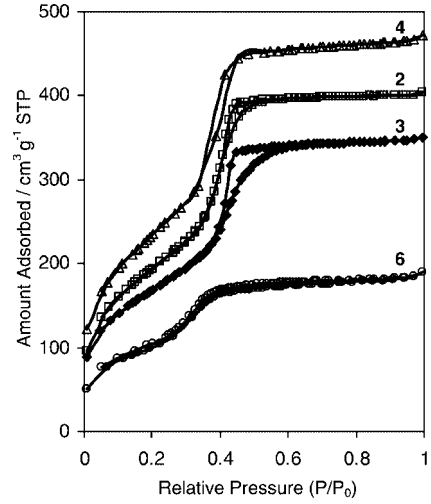

Figure 4. N_2 physisorption isotherms of solvent-extracted PMOs **2**–**4**, **6** (−□−, **2**; −♦−, **3**; −Δ−, **4**; −○−, **6**).

(49) (a) Kruk, M.; Jaroniec, M.; Sayari, A. *Langmuir* **1997**, *13*, 6267. (b) Zhao, D.; Yang, P.; Melosh, N.; Feng, J.; Chmelka, B. F.; Stucky, G. A. *Adv. Mater.* **1998**, *10*, 1380. (c) Kruk, M.; Jaroniec, M. *Chem. Mater.* **2001**, *13*, 3169. (d) Lukens, W. W., Jr.; Yang, P.; Stucky, G. D. *Chem. Mater.* **2001**, *13*, 28.

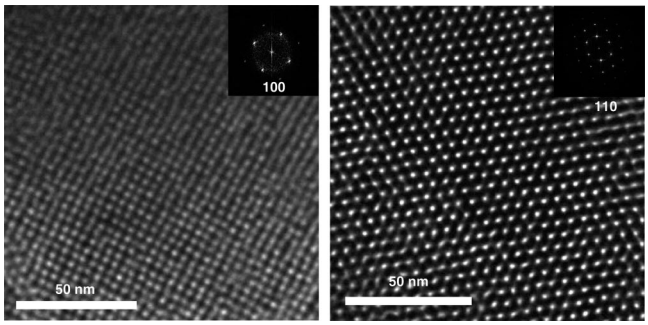

Figure 5. TEM images and Fourier diffractogram patterns for the solvent-extracted PMO **4** with *Fm*3*m* symmetry along [100] (left) and [110] (right) directions.

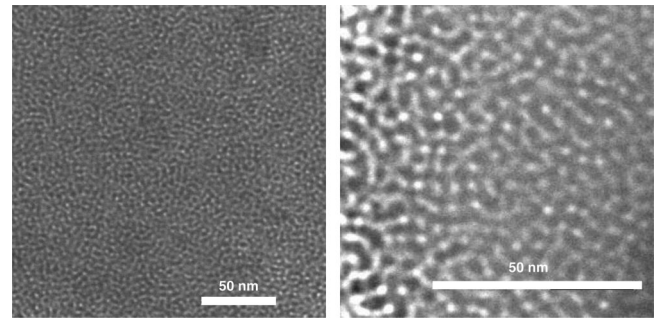

Figure 6. TEM images for the solvent-extracted PMO **6**.

5; SI, Figure S2). It is noteworthy that no intergrowths attributable to a 3D hexagonal phase were found along the [110] direction. In addition, the "twinned" hexagonal-close-packed structure can also be ruled out, since the Fourier diffractograms corresponding to the images taken along [110] show neither stacking faults nor streaking effects.[53–55] The absence of any other cage-type mesoporous materials, for example, with SBA-2, SBA-12, or FDU-1-type symmetry,[53–56] provided further evidence of the phase purity of the cubic PMO materials **3** and **4**. These results are in agreement with those of recently communicated PMOs with the *Fm*3*m* space group.[33]

Further increase of the molar ratio of NaOH to water gave sample **5**, the PXRD pattern of which indicates a distorted cubic structure (Figure 1). Next, PMO **6** was obtained at $NaOH/H_2O = 9.43 \times 10^{-3}$. Its broad PXRD peak, which was indexed as the (100) plane, confirmed a markedly decreased long-range ordering compared to samples **1**−**4**. TEM analysis proved the disordered three-dimensional network structure of PMO **6** featuring "wormholelike" mesoporous channels (Figure 6). An even further increase of the base concentration (molar ratio of $NaOH/H_2O > 9.43 \times 10^{-3}$) counteracted organosilica condensation and precipitation. These results imply that the NaOH concentration profile within the multicomposite BTEE−C_{18-3-1}/C_{16}TBr−NaOH−H_2O provides a convenient and efficient means for controlling the PMO mesophase.

The formation of a new mesophase structure in surfactant-containing multicomponent sol–gel synthesis is often difficult to interpret due to the complexity of the reaction processes. In general, the type/structure and concentration of the surfactant, (organo)silica precursor, pH value of the reaction mixture, reaction temperature, counterions, cosolvent, or organic additives synergistically affect the formation of the surfactant (template)/(organo)silica composite, and hence the structure of a given ordered periodic mesophase.[57] The shape/geometry of the surfactant micelles is especially important, and it is generally accepted that mesophase−mesophase transitions can be implied by changes of the surfactant interfacial curvature in the micelle.[15] This can be described by using the surfactant packing parameter (g) as $g = V/(a_0 l)$, where V is the total volume of surfactant chains plus any cosolvent organic molecule between the chains, a_0 is the effective hydrophilic headgroup area at the micelle interface, and l is the kinetic surfactant tail length or the curvature elastic energy. Accordingly, the value of g is codetermined by interfacial charge matching as well as by the packing of carbon chains. While the former is controlled by the pH value, cosolvent, and counterions, the latter is particularly affected by the reaction temperature and organic additives. Specific values of g are associated with inverted surfactant micelles ($g > 1$), lamellar phases ($g = 1$), vesicles ($1/2 < g < 1$), cylindrical micelles ($1/3 < g < 1/2$), and spherical micelles ($g < 1/3$). Lower g values generate large interfacial surface curvatures.[15] In the present reaction system, we observe a remarkable effect of the sodium hydoxide concentration; that is, a slight change of the base concentration ($Na^+OH^-/H_2O = 3.9 \times 10^{-3}$ to 9.43×10^{-3}; samples **1**−**6**) causes mesophase−mesophase transitions in the order hexagonal *p*6*mm* → cubic *Pm*3*n* → cubic *Fm*3*m* → distorted cubic phase → *MSU-type* structure. This can be qualitatively interpreted by charge-matching phenomena.[57] We suggest that the NaOH concentration controls the interactions and charge matching between the surfactant template and organosilica composite, which is driven by the ion exchange of organosilicate oligomers with Br^- or OH^-, leading to different values of g. At a low base concentration ($NaOH/H_2O = 3.89 \times 10^{-3}$), the binary surfactant mixtures prefer a packing structure with low surface curvature, which directs the formation of a stable hexagonal mesophase of the surfactant/organosilica composite. A higher base concentration ($4.32 \times 10^{-3} \leq NaOH/H_2O \leq 7.37 \times 10^{-3}$; SI, Figures S3 and S4) affects the aggregation/polycondensation of the hydrolyzed multihydroxyl organosilica and the overall negative charge of the resulting polyanionic organosilica. Simultaneously, the identical cationic surfactants repack to increase the effective headgroup area in order to compensate for the

(50) Kleitz, F.; Liu, D.; Anilkumar, G. M.; Park, I.-S.; Solovyov, L. A.; Shmakov, A. N.; Ryoo, R. *J. Phys. Chem. B* **2003**, *107*, 14296.
(51) Kleitz, F.; Solovyov, L. A.; Anilkumar, G. M.; Choi, S. H.; Ryoo, R. *Chem. Commun.* **2004**, 1536.
(52) (a) El-Safty, S. A.; Hanaoka, T. *Adv. Mater.* **2003**, *15*, 1893. (b) El-Safty, S. A.; Hanaoka, T. *Chem. Mater.* **2004**, *16*, 384.
(53) Hunter, H. M. A.; Garcia-Bennett, A. E.; Shannon, I. J.; Zhou, W.; Wright, P. A. *J. Mater. Chem.* **2002**, *12*, 20.
(54) Matos, J. R.; Kruk, M.; Mercuri, L. P.; Jaroniec, M.; Zhao, L.; Kamiyama, T.; Terasaki, O.; Pinnavaia, T. J.; Liu, Y. *J. Am. Chem. Soc.* **2003**, *125*, 821.
(55) Sakamoto, Y.; Díaz, I.; Terasaki, O.; Zhao, D.; Pérez-Pariente, J.; Kim, J. M.; Stucky, G. D. *J. Phys. Chem. B* **2001**, *106*, 3118.
(56) Zhou, W.; Hunter, H. M. A.; Wright, P. A.; Ge, Q.; Thomas, J. M. J. *Phys. Chem. B* **1998**, *102*, 6933.
(57) Monnier, A.; Schüth, F.; Huo, Q.; Kumar, D.; Margolese, D.; Maxwell, R. S.; Stucky, G. D.; Krishnamurty, M.; Petroff, P.; Firouzi, A.; Janicke, M.; Chmelka, B. F. *Science* **1993**, *261*, 1299.

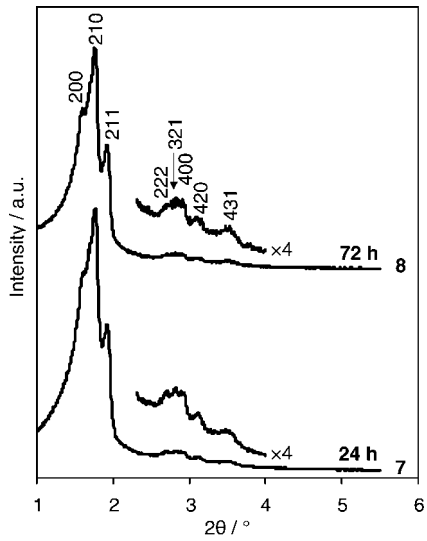

Figure 7. Powder X-ray diffraction patterns of solvent-extracted PMOs **7** and **8**.

overall changed negative charge of the organosilicate composite. This charge balancing results in a high interfacial surface curvature of the surfactant/organosilicate aggregate involving a larger value of a_0 and, hence, a smaller g value, which drives the *p*6*mm* → *Pm*3*n* → *Fm*3*m* mesophase transformation. A further increase of the base concentration might lead to a partial breakup ($NaOH/H_2O = 7.37 \times 10^{-3}$) and finally a complete reorganization of the uniform binary surfactant packing structure ($NaOH/H_2O = 9.43 \times 10^{-3}$), causing the formation of a distorted cubic mesophase and hexagonal *MSU-type* mesophase, respectively. Accordingly, for the various organosilica mesophases formed in the $C_{16}TABr/C_{18-3-1}$ binary surfactant mixtures under basic conditions, the surface curvature of the micellar assemblies increased in the following order: hexagonal *MSU-type* ≤ hexagonal (*p*6*mm*) < cubic (*Pm*3*n*) < face-centered cubic (*Fm*3*m*). This order is in complete accordance with that reported by El-Safty and Hanaoka[52] and Tiddy et al.[58] in acidic nonionic surfactant micellar systems. Hence, the change of the base concentration can be viewed as a switch to effectively control mesophase transformations.

N_2 physisorption proved to be a valuable tool to investigate the pore configuration of periodic mesoporous architectures. The adsorption–desorption isotherms of materials **3**−**6** exhibit type-IV characteristics (Figure 4; for clarity reasons, the isotherm for material **5** is not shown). For PMO **3**, a clear H2 hysteresis loop is observed, typical of mesoporous materials with cagelike pores.[49] Material **6** displays a comparatively small specific BET surface area, pore diameter, and pore volume. BJH analyses revealed a narrow pore size distribution for all PMOs indicative of well-defined uniform pores (SI, Figure S5).

For comparison, the replacement of divalent surfactant C_{18-3-1} by C_{16-3-1} in the otherwise identical synthesis mixture used for PMO **4** gave material **7**, the mesophase of which was verified as cubic *Pm*3*n* by PXRD analysis (Figure 7) and TEM (Figure 8). This mesophase transformation also qualitatively reflects the change of the surfactant packing parameter. The overall shorter tail length of the binary surfactants implicates a higher special g value, which results in the formation of a mesoporous organosilica material **7** with lower surface interfacial curvature (*Pm*3*n* < *Fm*3*m*).

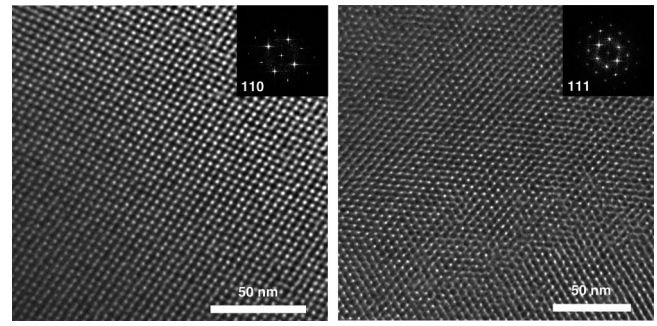

Figure 8. TEM images and Fourier diffractogram patterns for the solvent-extracted PMO **7** with *Pm*3*n* symmetry along [110] (left) and [111] (right) directions.

Increase of the aging time from 24 to 72 h under otherwise identical synthesis conditions produced PMO **8**, which exhibited a better long-range ordering as demonstrated by PXRD (Figure 7) and TEM analysis (SI, Figure S2). Such well-ordered pores along the [110], [111], and [210] incidences suggest a precise periodicity of 3D cubic *Pm*3*n* symmetry (cf., purely siliceous SBA-1).[48] However, with prolonged aging time, the mesophase structure and the type of nitrogen gas physisorption isotherm did not undergo any significant changes (SI, Figure S6; Table 2). This finding implies that, for cubic *Pm*3*n* materials, extension of the aging time is not a proper means for changing the material's physical properties. This can be explained by the high stability of such cubic PMO frameworks, which impedes a 3D enlargement of the mesopores. This finding is also confirmed by the hydrothermal stability of cagelike PMOs (see below).

The cage diameter D_{me} of samples **2**, **3**, **4**, **7**, and **8** was calculated by using eq 1 (Table 2).[47] Accordingly, the D_{me} of cubic mesoporous materials mainly depends on the nature of the mesophase and physical parameters, such as pore volume and unit cell parameters. It is noteworthy that the use of surfactant C_{16-3-1} instead of C_{18-3-1} resulted in significantly smaller cages (D_{me} = 55 versus 60 Å). Complete removal of the surfactant molecules and the structural integrity of the $SiO_{1.5}-CH_2-CH_2-SiO_{1.5}$ framework of the PMOs was confirmed by ^{13}C cross-polarization and ^{29}Si MAS NMR spectroscopy (spectra of PMO **4**: SI, Figure S7).[26,38,59]

SEM images of PMOs **1**−**8** revealed various crystal-like morphologies (Figure 9 and Figure S8 in the SI). While hexagonal PMO **1** is composed of small spheres and larger ellipsoids (∼2 μm) (Figure 9A), uniform and regular shapes with square and hexagonal faces (∼3 μm) were found for cubic PMO **2** (SI, Figure S8A). Material PMO **3** (cubic *Fm*3*m* symmetry) obtained at a relatively low NaOH concentration consists of aggregated coarse particles without

(58) Sakya, P.; Seddon, J. M.; Templer, R. H.; Mirkin, R. J.; Tiddy, G. J. T. *Langmuir* **1997**, *13*, 3706.

(59) McInall, M. D.; Scott, J.; Mercier, L.; Kooyman, P. J. *Chem. Commun.* **2001**, 2282.

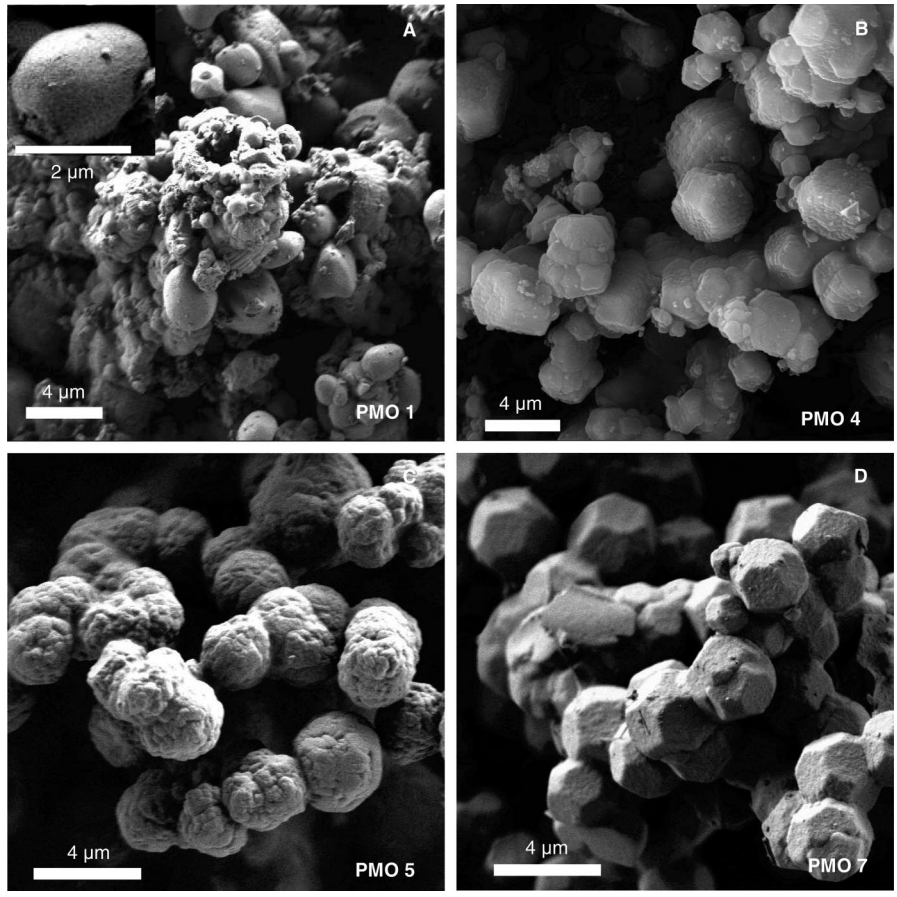

Figure 9. SEM images for PMOs **1** (A), **4** (B), **5** (C), and **7** (D).

well-defined external morphology (SI, Figure S8B). Higher base concentrations gave truncated-cube features with small hexagonal faces along with slice aggregation (PMO **4**; Figure 9B), or uniform spherical particles ($\sim 3\ \mu$m) with a coarse external surface (PMO **5**, Figure 9C). The wormholelike mesophase **6** does not exhibit a regular morphology (SI, Figure S8C). In contrast, PMOs **7** and **8** feature well-defined particle morphologies (Figure 9D; SI, Figure S8D) comprising decaoctahedrons with 6 squares and 12 hexagons, that is, a cube whose edges are truncated by hexagons. Four 3-fold axes with cubic symmetry were clearly observed, and the squares and hexagons were indexed as (100) and (110) planes, respectively.[26,48]

Hydrothermal stability seems to be a peculiar feature of template-extracted PMOs, which could make them superior to purely siliceous PMS materials for various applications. The hydrothermal stability of PMOs with hexagonal symmetry has been demonstrated previously (a) in the presence of aluminum[60] and (b) for the utilization of both cationic[61,62] and neutral surfactants.[63,64] We selected three of our PMO materials with different symmetries (*Pm*3*n*, *Fm*3*m*, and *p*6*mm*) to carry out a similar hydrothermal stability test by treating the materials in water at 100 °C for various time periods. The PXRD patterns indicated the absence of any structural degradation for the cagelike PMOs **2** and **3** after hydrothermal treatment (Figure 10). For cubic PMO **3** with *Fm*3*m* symmetry, hydrothermal treatment for 24 (**3a**) and 72 h (**3b**) markedly increased the intensities of the (111) and (200) reflections, with the peaks slightly shifted to higher 2θ angles. The intensity of the (200), (220), and (311)

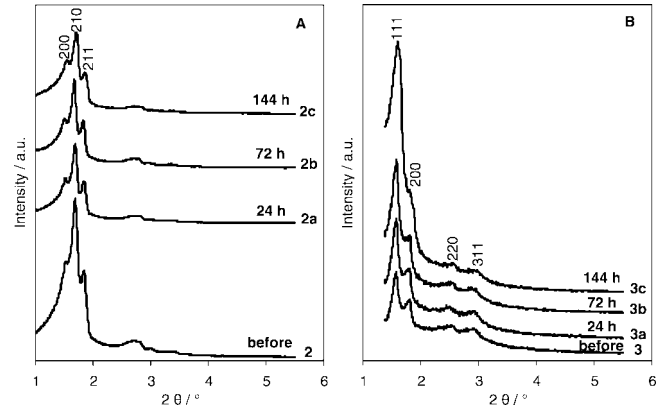

Figure 10. Powder X-ray diffraction patterns of cubic PMOs **2**−**2c** with *Pm*3*n* symmetry (A) and cubic PMOs **3**−**3c** with *Fm*3*m* symmetry (B) before and after hydrothermal treatment.

(60) (a) Xia, Y.; Wang, W.; Mokaya, R. *J. Am. Chem. Soc.* **2005**, *127*, 790. (b) Guo, W.; Zhao, X. S. *Microporous Mesoporous Mater.* **2005**, *85*, 32.
(61) Matsumoto, A.; Misran, H.; Tsutsumi, K. *Langmuir* **2004**, *20*, 7139.
(62) (a) Xia, Y.; Mokaya, R. *Microporous Mesoporous Mater.* **2005**, *86*, 231. (b) Shylesh, S.; Jha, R. K.; Singh, A. P. *Microporous Mesoporous Mater.* **2006**, *94*, 364.
(63) Burleigh, M. C.; Markowitz, M. A.; Jayasundera, S.; Spector, M. S.; Thomas, C. W.; Gaber, B. P. *J. Phys. Chem. B* **2003**, *107*, 12628.
(64) (a) Cho, E.-B.; Char, K. *Chem. Mater.* **2004**, *16*, 270. (b) Liu, J.; Yang, Q.; Kapoor, M. P.; Setoyama, N.; Inagaki, S.; Yang, J.; Zhang, L. *J. Phys. Chem. B* **2005**, *109*, 12250. (c) Guo, W.; Li, X.; Zhao, X. S. *Microporous Mesoporous Mater.* **2006**, *93*, 285.

reflections increased even more for material **3c** (144 h), albeit the (200) peak was only indicated by a shoulder. For hexagonal PMO **9**, we observed a considerable decrease of the intensities of the (100), (110), and (200) reflections after 24 h (**9a**), however, which regained intensity after 72 (**9b**) and 144 h (**9c**) (SI, Figure S10).[61,63]

Nitrogen physisorption analyses were performed on all of the hydrothermally treated PMOs, revealing the preservation of the type-IV isotherms including distinct features such as hysteresis loops (SI, Figures S9 and S10). Detailed physicochemical parameters of the PMOs after hydrothermal treatment are listed in Table S1 (SI). It is noteworthy that for all of the cubic PMOs the pore diameter slightly increased and the pore wall thickness slightly decreased. This is attributed to dissolution of the pore walls during extensive treatment in boiling water. For cubic PMOs with *Fm*3*m* symmetry, hydrothermal post-treatment for 144 h caused a significantly decreased BET surface area, pore volume, and pore wall thickness, which is in accordance with the X-ray data.

Previous reports have revealed that purely siliceous PMS materials, and in particular hexagonal MCM-41, suffer a major collapse of the mesopore structure in boiling water after 18 h or at ambient temperature after 10 months.[65–67] Our investigations are in agreement with those reported previously for PMOs with different bridging groups.[61,63] Correspondingly, we suggest that the high hydrothermal stability of PMO materials is most likely attributed to the low polarity or high hydrophobicity of the PMO surface. The bridging organic (ethylene) groups which are uniformly distributed in the inorganic framework effectively hamper the adsorptive interaction between water and the surface of PMOs, thus retarding the hydrolysis of the siloxane framework.

Conclusions

Ethylene-bridged periodic mesoporous organosilicas of distinct hexagonal and cubic symmetries (*p*6*mm*, *Pm*3*n*, *Fm*3*m, MSU-type*) are accessible straightforwardly from the multicomposite BTEE−C_{18-3-1}/C_{16}TABr−NaOH−H_2O by slight variations of the NaOH concentration profile. The appearance of these mesophase−mesophase transitions can be interpreted qualitatively by changes of the surfactant interfacial curvature in the micelle (surfactant packing parameter *g*) and adherence to the charge-matching principle. This is supported by emerging phase transformations upon simply changing the tail length of the divalent surfactant under otherwise identical synthesis conditions (C_{18-3-1}, *Fm3m*; C_{16-3-1}, *Pm3n*). Given the high hydrothermal stability and the occurrence of regular morphologies (SEM), such cagelike organosilicas qualify for many applications including size-exclusive separation processes, size-selective catalysis, enzyme immobilization, and drug delivery.

Acknowledgment. This work was supported by the Deutsche Forschungsgemeinschaft, the Fonds der Chemischen Industrie, and the NANOSCIENCE program of the University of Bergen. The authors are grateful to Dr. G. Raudaschl-Sieber for recording the solid-state NMR spectra.

Supporting Information Available: PXRD patterns, nitrogen physisorption isotherms, TEM and SEM images, as well as MAS NMR spectra of the materials under study (Figures S1−S10); Table S1 listing the structural properties of extracted PMOs before and after the hydrothermal stability test. This material is available free of charge via the Internet at http://pubs.acs.org.

CM702359R

(65) Landau, M. V.; Varkey, S. P.; Herskowitz, M.; Regev, O.; Pevzner, S.; Sen, T.; Luz, Z. *Microporous Mesoporous Mater.* **1999**, *33*, 149.
(66) Ribeiro Carrott, M. M. L.; Estêveão Candeias, A. J.; Carrott, P. J. M.; Unger, K. K. *Langmuir* **1999**, *15*, 8895.
(67) Broyer, M.; Valange, S.; Bellat, J. P.; Bertrand, O.; Weber, G.; Gabelica, Z. *Langmuir* **2002**, *18*, 5083.